Plasma Science and Technology

Screening effect of plasma flow on the resonant magnetic perturbation penetration in tokamaks based on two-fluid model

Weikang TANG (汤炜康)[1,2] , **Qibin LUAN** (栾其斌)[3,*], **Hongen SUN** (孙宏恩)[3],
Lai WEI (魏来)[1,2], **Shuangshuang LU** (路爽爽)[1], **Shuai JIANG** (姜帅)[1],
Jian XU (徐健)[1] **and Zhengxiong WANG** (王正汹)[1]

[1] Key Laboratory of Materials Modification by Laser, Ion, and Electron Beams (Ministry of Education),
School of Physics, Dalian University of Technology, Dalian 116024, People's Republic of China
[2] Key Laboratory of Geospace Environment, University of Science and Technology of China, Hefei
230026, People's Republic of China
[3] Faculty of Electronic Information and Electrical Engineering, Dalian University of Technology, Dalian
116024, People's Republic of China

E-mail: luanqb@dlut.edu.cn

Abstract
Numerical simulation on the resonant magnetic perturbation penetration is carried out by the
newly-updated initial value code MDC (MHD@Dalian Code). Based on a set of two-fluid four-
field equations, the bootstrap current, parallel, and perpendicular transport effects are included
appropriately. Taking into account the bootstrap current, a mode penetration-like phenomenon is
found, which is essentially different from the classical tearing mode model. To reveal the
influence of the plasma flow on the mode penetration process, $\mathbf{E} \times \mathbf{B}$ drift flow and diamagnetic
drift flow are separately applied to compare their effects. Numerical results show that a
sufficiently large diamagnetic drift flow can drive a strong stabilizing effect on the neoclassical
tearing mode. Furthermore, an oscillation phenomenon of island width is discovered. By
analyzing it in depth, it is found that this oscillation phenomenon is due to the negative feedback
regulation of pressure on the magnetic island. This physical mechanism is verified again by key
parameter scanning.

(Some figures may appear in colour only in the online journal)

1. Introduction

Tearing mode (TM) instability has been extensively investigated
by researchers in the area of tokamak plasmas in recent decades
[1, 2]. The TM is one kind of current-driven magnetohydro-
dynamic (MHD) instability commonly followed by magnetic
reconnection, which can break up the nested magnetic flux sur-
faces and generate magnetic islands at the corresponding resonant
surface. These magnetic islands can provide a 'seed', called a
seed island, for the neoclassical tearing mode (NTM) to grow.
NTM, a pressure gradient-driven MHD instability, is linearly
stable but can be destabilized by helical perturbations due to the
loss of bootstrap current inside the seed island [3]. The onset of
NTM is the principal limitation of the plasma temperature in the
core region [4], owing to the radial 'shortcut' transport in the
produced large magnetic island, and one of the main causes of
major disruption [5, 6]. For the sake of economic feasibility, a
high fraction of bootstrap current, up to 80%–90%, is required
for a future advanced tokamak. Since NTM is a high beta
phenomenon, which is proportional to the bootstrap current
fraction, the control and suppression of NTM are of great sig-
nificance for the steady-state operation of tokamak devices [7–9].

Aiming to control the NTM, many research efforts have
been dedicated to resonant magnetic perturbation (RMP)

[10–16]. RMP has been found to drive additional effects on magnetic islands in tokamak plasmas. Specifically, the RMP can produce an electromagnetic torque at the corresponding resonant surface. Once the electromagnetic torque is sufficiently large to balance the plasma viscosity and inertia torque, the magnetic islands would be compulsorily aligned with the RMP in an identical frequency, called locked mode (LM) [17]. For a static RMP, it can be used to test the maximum tolerance for the residual error field, resulting from the asymmetry of the tokamak device [18]. As for the dynamic RMP, it can be utilized to unlock the magnetic island and maintain a stable toroidal and poloidal rotation [19]. Lately, experimental and numerical results show that the synergetic application of RMP and electron cyclotron current drive (ECCD) is a promising and effective method to control the NTM [20–22]. The RMP can be used as an auxiliary method to lock and locate the phase of the NTM, and then to enhance the accuracy and effectiveness of the ECCD.

In addition to the above application, even if the rotating plasma is originally stable to the NTM, the RMP can drive magnetic reconnection and generate a magnetic island at the resonant surface, called mode penetration [23, 24]. Mode penetration has raised many concerns since its threshold is directly related to the onset of TM/NTM. Based on single-fluid theory, considerable studies have been made in predicting and explaining the threshold of mode penetration for different tokamak devices [12, 25–28] and parameter regimes [29–32]. However, considering the plasma rotation playing a significant role in the screening process of RMP [33], the two-fluid model, retaining the electron diamagnetic drift as well as the $\mathbf{E} \times \mathbf{B}$ flow, is more suitable to account for more complex physics. Recently, in the frame of the two-fluid drift-MHD theory, plenty of research was carried out to investigate the interaction of the RMP and magnetic islands in tokamak plasmas [34–36]. Using a two-fluid model, Hu *et al* found that the two-fluid effects can give significant modifications to the scaling law of mode penetration for different plasma parameters. Besides, the enduring mystery, a non-zero penetration threshold at zero plasma natural frequency, is explained by the small magnetic island width when penetrated [37, 38]. In the recent investigation, numerical results show that the 2/1 NTM can be suppressed by the 4/2 RMPs with moderate amplitudes if the bi-normal fluid rotation frequency is in the ion diamagnetic drift direction or sufficiently large [39].

Motivated by the above reasons, based on the two-fluid model, the screening effects of two components of plasma flow on mode penetration are investigated in this work. Taking into account the bootstrap current, a mode penetration-like process is found by numerical simulation. Furthermore, it is found that the diamagnetic drift flow has a stabilizing effect on the magnetic islands. An oscillation phenomenon of island width is discovered in the high Lundquist number S and high transport scenario.

The rest of this paper is organized as follows. In section 2, the modeling equations used in this work are introduced. In section 3, numerical results and physical discussions are presented. Finally, the paper is summarized and conclusions are drawn in section 4.

2. Physical model

The initial value code MDC (MHD@Dalian Code) [40–46] is upgraded to the two fluid versions based on a set of four-field MHD equations [47]. Taking into account the nonlinear evolution of the vorticity U, the poloidal magnetic flux ψ, the plasma pressure p, and the parallel ion velocity v, the normalized equations in the cylindrical geometry (r, θ, z) can be written as

$$\frac{\partial U}{\partial t} = [U, \phi + \delta\tau p] + \nabla_{\parallel} j + \nu \nabla_{\perp}^2 U + \delta\tau [\nabla_{\perp} p, \nabla_{\perp} U],$$
(1)

$$\frac{\partial \psi}{\partial t} = -\nabla_{\parallel} \phi + \delta \nabla_{\parallel} p - \eta(j - j_{\mathrm{b}}),$$
(2)

$$\frac{\partial p}{\partial t} = [p, \phi] + 2\beta_{\mathrm{e}} \delta \nabla_{\parallel} j - \beta_{\mathrm{e}} \nabla_{\parallel} v + \chi_{\parallel} \nabla_{\parallel}^2 p + \chi_{\perp} \nabla_{\perp}^2 p,$$
(3)

$$\frac{\partial v}{\partial t} = [v, \phi] - \frac{1}{2}(1 + \tau)\nabla_{\parallel} p + \mu \nabla_{\perp}^2 v,$$
(4)

where ϕ and j are, respectively, the electric potential and plasma current density along the axial direction, obtained by the following formulas $U = \nabla_{\perp}^2 \phi$ and $j = -\nabla_{\perp}^2 \psi$. The equation (1) (vorticity equation) is the perpendicular component (taking $e_z \cdot \nabla \times$) of the equation of motion, where ν is the viscosity and $\tau = T_{\mathrm{i}}/T_{\mathrm{e}}$ is the ratio of ion to electron temperature. $\delta = (2\Omega_{\mathrm{i}}\tau_{\mathrm{a}})^{-1}$ is a gyroradius parameter, where $\Omega_{\mathrm{i}} = eB_0/m_{\mathrm{i}}$ is a constant measure of the ion gyrofrequency and $\tau_{\mathrm{a}} = \sqrt{\mu_0 \rho} \, a/B_0$ is Alfvén time. Neglecting the electron inertia and Hall effect, equation (2) is obtained by combining the generalized Ohm's law and Faraday's law of electromagnetic induction, where η is the resistivity. $j_{\mathrm{b}} = -(A\sqrt{\varepsilon}/B_{\theta})p'(r)$ is the bootstrap current [48], where $\varepsilon = a/R_0$ is the inverse aspect ratio, and B_{θ} is the poloidal magnetic field. A is a constant that can be calculated by a given bootstrap current fraction $f_{\mathrm{b}} = \int_0^a j_{\mathrm{b}} r \mathrm{d}r / \int_0^a jr \mathrm{d}r$. Since the isothermal assumption is made here, the evolution of pressure is mainly determined by the particle conservation law. It is basically a transport equation, considering the convective term, parallel and perpendicular heat transport. By including the effect of resistive diffusion and the parallel ion flow, equation (3) is the final energy transport equation for two-fluid plasma. $\beta_{\mathrm{e}} = 2\mu_0 n_0 T_{\mathrm{e}}/B_0^2$ is the electron plasma beta at the location of the magnetic axis, where T_{e} is the constant electron temperature. $\chi_{\parallel}$ and $\chi_{\perp}$ are the parallel and perpendicular transport coefficients, respectively. The equation (4) is the parallel component of the equation of motion by taking the dot product of the equation with B, where μ is the diffusion coefficient of parallel ion velocity. This model can reduce to the high-beta reduced MHD equations of Strauss [49], by giving the limit $\delta \to 0$, $\beta_{\mathrm{e}} \to 0$. New physics appears by introducing the two factors δ, measuring the finite Larmor radius (FLR) effects, and β_{e}, measuring the compressibility. If one has $\delta \to 0$ and $T_{\mathrm{i}} = T_{\mathrm{e}}$, but non-zero β_{e}, the model reduces to the compressible reduced MHD (CRMHD) equations [50].
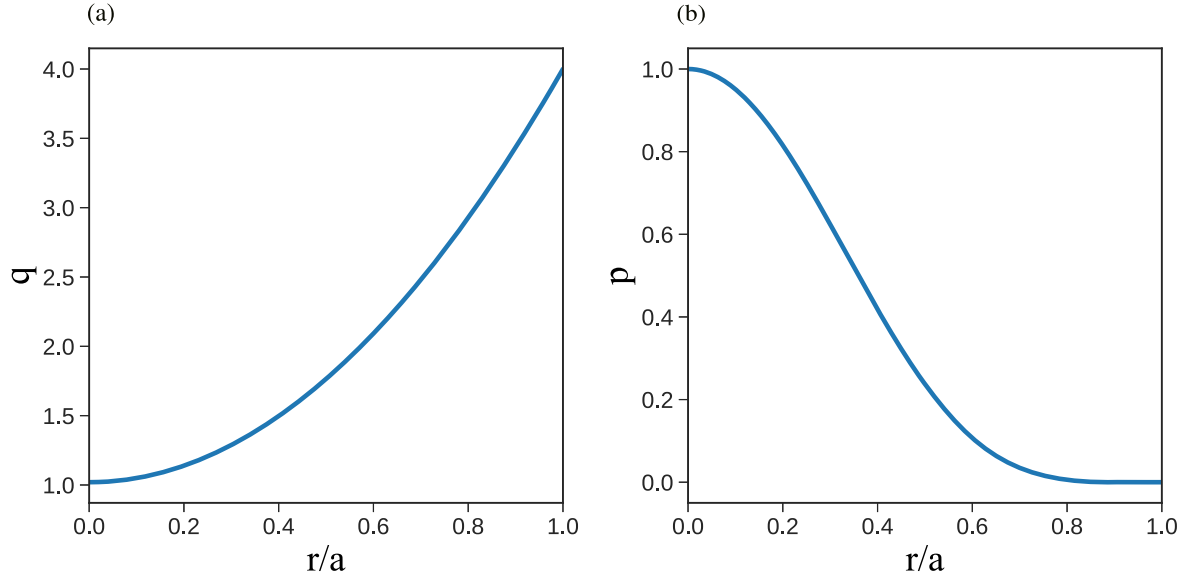
Figure 1. Safety factor q and pressure p profiles adopted in this work.

The length l, time t, and velocity v are normalized by the minor radius a, Alfvén time τ_a and Alfvén speed $v_a = B_0/\sqrt{\mu_0 \rho}$, respectively. The poloidal magnetic flux ψ, electric potential ϕ and plasma pressure p are normalized by aB_0, $aB_0 v_a$ and the pressure at the magnetic axis, respectively. The normalization of the diffusion coefficients is as follows, η, ν, μ, $\chi_\parallel$, $\chi_\perp$ are normalized by $\mu_0 a^2/\tau_a$, a^2/τ_a, a^2/τ_a, a^2/τ_a, a^2/τ_a, respectively. The Poisson brackets in equations (1)–(4) are defined as

$$[f, g] = \nabla f \times \nabla g \cdot \hat{z} = \frac{1}{r}\left(\frac{\partial f}{\partial r}\frac{\partial g}{\partial \theta} - \frac{\partial g}{\partial r}\frac{\partial f}{\partial \theta}\right). \qquad (5)$$

Each variable $f(r, \theta, z, t)$ in equations (1)–(4) can be written in the form $f = f_0(r) + \widetilde{f}(r, \theta, z, t)$ with f_0 and $\widetilde{f}$ being the time-independent initial profile and the time-dependent perturbation, respectively. By applying the periodic boundary conditions in the poloidal and axial directions, the perturbed fields can be Fourier-transformed as

$$\widetilde{f}(r, \theta, z, t) = \frac{1}{2}\sum_{m,n}\widetilde{f}_{m,n}(r, t)e^{im\theta - inz/R_0}, \qquad (6)$$

with R_0 being the major radius of the tokamak, m and n being the poloidal and toroidal mode number, respectively.

The effect of RMP with m/n is taken into account by the boundary condition

$$\widetilde{\psi}_{m,n}(r = 1) = \psi_a(t)e^{im\theta - inz/R_0}. \qquad (7)$$

In this way, the perturbed radial magnetic field at the plasma boundary over the toroidal magnetic field could be calculated by $\delta B_r/B_0 = am\psi_a$. It should be pointed out that, in a real tokamak, the toroidal rotation is prevailing and much stronger than the poloidal one, whereas only the poloidal rotation is considered in this work. Considering the fact that the electromagnetic force exerted in the poloidal direction is $(n/m)(r_s/R)$ times smaller than that in the toroidal direction, where r_s is the radial location of the resonant surface, and the speed in the toroidal direction should be $(m/n)(R/r_s)$

times larger than the poloidal one for having an equivalent rotation frequency, the locking threshold in the toroidal direction can, therefore, be estimated by multiplying such a factor $[(m/n)(R/r_s)]^2$.

Given the initial profiles of ϕ_0, ψ_0, p_0 and v_0, equations (1)–(4) can be solved simultaneously by our code MDC. The two-step predictor-corrector method is applied in the time advancement. The finite difference method is used in the radial direction and the pseudo-spectral method is employed for the poloidal and the toroidal directions (θ, $\zeta = -z/R_0$).

3. Simulation results

3.1. Numerical set-up

Considering a low-density ohmically heated tokamak discharge with electron density $n_e \approx 2 \times 10^{19}\,\mathrm{m}^{-3}$, toroidal magnetic field $B_0 = 2$ T and $\varepsilon = 0.25$, this will lead to the Alfvén speed $v_a \approx 6.9 \times 10^6\,\mathrm{m\,s}^{-1}$ and Alfvén time $\tau_a \approx 7.24 \times 10^{-8}$ s. The corresponding Alfvén frequency is $\omega_a \approx 1.38 \times 10^7$ Hz. Otherwise stated, other plasma parameters are set as follows, $\tau = 1$, $\beta_e = 0.01$, $\eta = 10^{-6}$, $\nu = 10^{-7}$, $\mu = 10^{-6}$, $\chi_\parallel = 10$ and $\chi_\perp = 5 \times 10^{-6}$. In the experimental condition, $\chi_\parallel/\chi_\perp$ can be 10^8–10^{10}. However, in our simulation, this value is a little lower than the realistic one due to computational limitations. The radial mesh number is set as $N_r = 2048$. The typical time step Δt in the simulations is chosen as 0.001. However, Δt varies from different cases due to numerical stability. In this work, the nonlinear simulations only include single helicity perturbations with higher harmonics ($m/n = 3/2$, $3 \leqslant m \leqslant 18$), in addition to the changes in the equilibrium quantities ($m/n = 0/0$ component). To simulate the mode penetration process, a linearly stable equilibrium safety factor q profile and the normalized plasma pressure p profile $p_0(r) = (1 - r^2)^5$ are given in figure 1, with the $q = 3/2$ resonant surface located at $r = 0.402$.
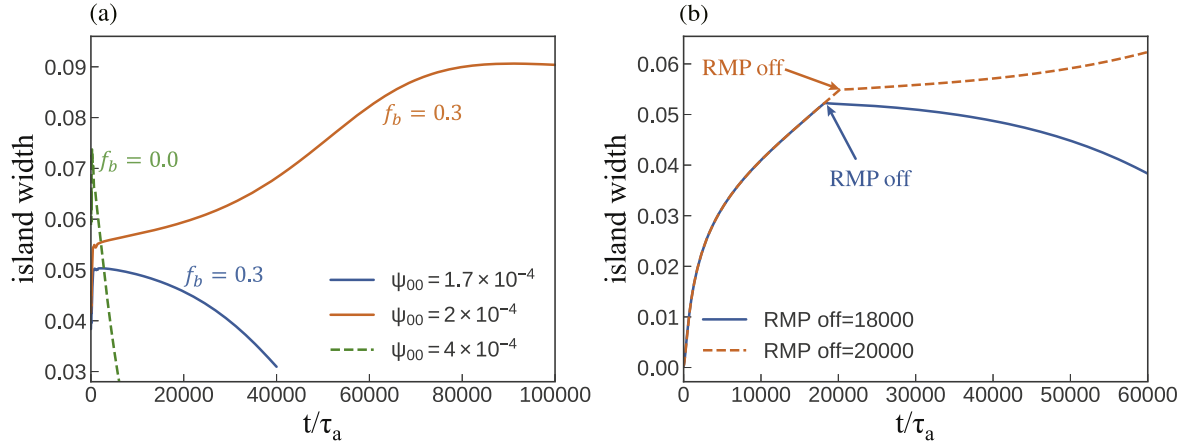
Figure 2. (a) Nonlinear evolution of the island width for different magnitudes of seed island. The solid traces are for bootstrap current fraction $f_b = 0.3$ and the dashed trace is for $f_b = 0$. (b) Nonlinear evolution of island width for different turn-off times of RMP with $f_b = 0.3$ and $\delta B_r/B_0 = 3.75 \times 10^{-5}$.
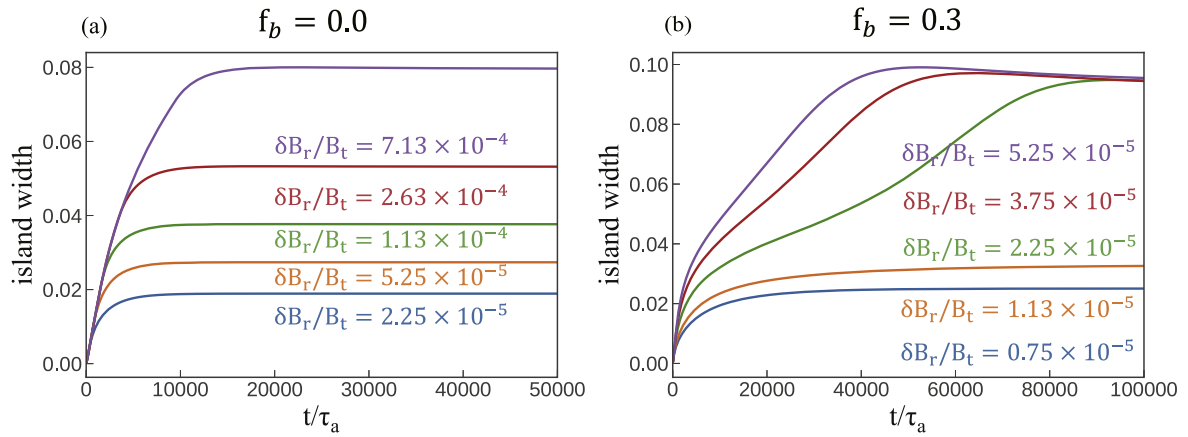
Figure 3. Temporal evolutions of island width for different RMP amplitudes for bootstrap current fraction $f_b = 0$ (a) and $f_b = 0.3$ (b) without plasma rotation.

3.2. Basic verification

To begin with, the role of seed island width on the onset of NTM is verified to ensure the neoclassical current effect is implemented properly. Under real experimental conditions, the seed island comes from a variety of sources, and it may come from different MHD modes, so the seed island width is considered by the initial magnetic perturbation in an arbitrary form of $\widetilde{\psi}_{t=0} = \psi_{00}(1 - r)^2$. The nonlinear evolution of magnetic island width for different initial magnetic perturbations is presented in figure 2(a). The solid traces are for bootstrap current fraction $f_b = 0.3$ (NTM) and dotted one for $f_b = 0.0$ (TM). For the classical TM, even if a very large seed island width is given, the island width still fades with time, illustrating that the TM in this q profile is linearly stable. Taking the bootstrap current into consideration, it is seen that there is a threshold for the mode to grow, manifesting that the nonlinearly unstable NTM is triggered for a larger seed island width. In experiments, the RMP coils are commonly used to seed a magnetic island. Then the onset of NTM by RMP is tested ($\widetilde{\psi}_{t=0} = 0$). The RMP is turned on from the very beginning with the amplitude of $\delta B_r/B_0 = 3.75 \times 10^{-5}$. In

figure 2(b), in the presence of RMP, the nonlinear evolution of island width for $f_b = 0.3$ is shown. After applying the RMP, the originally stable TM can be driven unstable, as the island width grows even without seed island. Then the RMP is turned off at different times when island width grows to a moderate magnitude, to testify if it is the driven reconnection or the onset of NTM. It turns out that, if the RMP is turned off before the island width is sufficiently large, the magnetic island still could not grow spontaneously. It confirms again the existence of the critical island width for triggering the NTM, which is consistent with the theory.

### 3.3. Effects of electric drift flow

Based on the above results, the effects of different RMP amplitudes are then scanned for $f_b = 0.0$ and $f_b = 0.3$ with zero rotation (electric drift ω_E and diamagnetic drift ω_{dia} are both zero). For $f_b = 0.0$ (figure 3(a)), the saturated island width is positively related to the RMP amplitude, a typical driven reconnection. However, for $f_b = 0.3$ (figure 3(b)), a mode penetration like phenomenon can be observed. If the RMP amplitude is relatively small, the magnetic island is going to
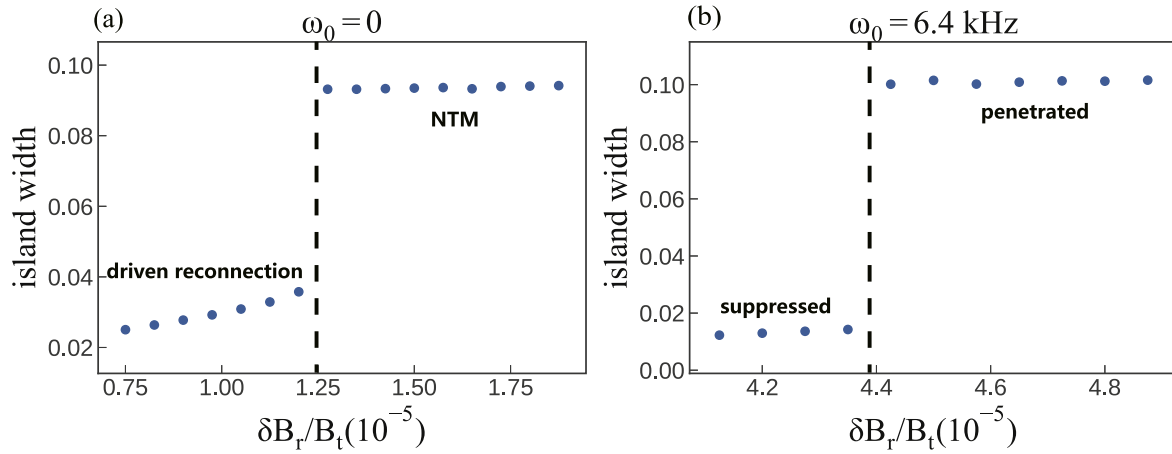
Figure 4. Island width versus the RMP amplitude for natural frequency $\omega_0 = 0$ (a) and $\omega_0 = 6.4$ kHz (b). The bootstrap current fraction f_b is set as 0.3.

saturate at a very small magnitude. Once the RMP amplitude is sufficiently large, the final island width would be very large and keep almost the same even further increasing the RMP amplitude. On the other hand, this phenomenon is different from the so-called mode penetration, and we will demonstrate it next.

Corresponding to figure 3(b), the saturated magnetic island width is shown as a function of RMP amplitude in figure 4(a). As the RMP amplitude increases, the saturated island width increases slowly first. Once the RMP amplitude exceeds a threshold, there is a jump in the saturated island width. This process can be divided into two parts, i.e. the driven reconnection phase for smaller RMPs and the onset of NTM for large RMPs. Next, including the effect of equilibrium $\mathbf{E} \times \mathbf{B}$ flow, a scan over the RMP amplitude is performed again. The equilibrium $\mathbf{E} \times \mathbf{B}$ flow is considered by a poloidal momentum source $\Omega_s(r) = 1/r^* \mathrm{d}\phi_0/\mathrm{d}r$. Here, δ is set to be zero, so only the $\mathbf{E} \times \mathbf{B}$ flow is considered. For a 6.4 kHz plasma rotation, the saturated island width versus the RMP amplitude is presented in figure 4(b). This is a typical mode penetration case, as the RMP amplitude increases above a threshold, the island width boosts to a large magnitude. There is one main distinction between figures 4(a) and (b), even though they look similar. That is, below the threshold, the island width barely changes for the case with plasma rotation but slowly increases for the case without rotation. The increase regime for the case without rotation is due to the forced reconnection driven by the externally applied RMP. However, the regime below the threshold for the case with rotation is due to the screening effect of the plasma flow. The corresponding eigenmode structures of perturbed poloidal magnetic flux and current density for the case without/with plasma rotation are plotted in figure 5. It can be clearly observed that the RMP is screened inside the resonant surface for the case with rotation, from the fact that the magnetic perturbation is nearly zero for $r < r_s$. In addition, a strong shielding current is formed at the resonant surface, which is consistent with the results on TEXTOR tokamak [51]. These characteristics are the same as the small locked island phenomenon in [52, 53], suggesting that the small locked island is the complete suppression of the magnetic island by
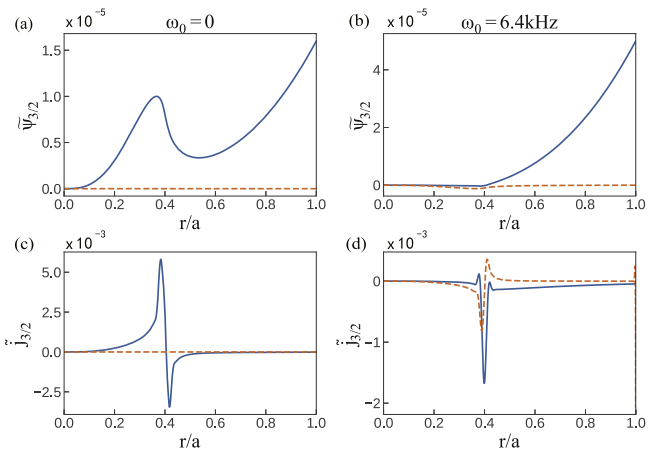
Figure 5. The typical eigenmode structure of poloidal magnetic flux and current density for $m/n = 3/2$ component in the regime below the jump of island width. For natural frequency $\omega_0 = 0$ (a) and (c), the magnetic perturbation in the core region is excited by the RMP. For $\omega_0 = 6.4$ kHz (b) and (d), the RMP is kept out from the resonant surface. The solid traces are for the real part and the dashed traces are for the imaginary part.

the RMP. Besides, a recent study also shows similar feasibility of magnetic island suppression by RMP at moderate amplitude [54]. For the case without rotation, on the other hand, the $m/n = 3/2$ component of magnetic perturbation is induced and kept by the 3/2 RMP at the boundary, indicating that mode penetration has already taken place.

All in all, the above simulation results suggest that, without plasma flow, the penetration threshold for the RMP is zero. Considering the effect of bootstrap current, however, the onset of NTM can lead to a mode penetration-like phenomenon, a driven connection regime plus an NTM regime. As a result, it seems that there is a finite threshold for mode penetration if not carefully distinguished.

3.4. Effects of diamagnetic drift flow

In this subsection, the effects of diamagnetic drift flow on the RMP penetration are numerically studied in comparison with
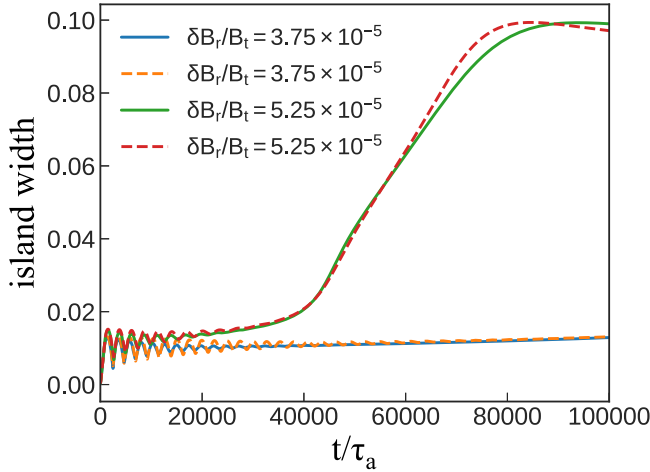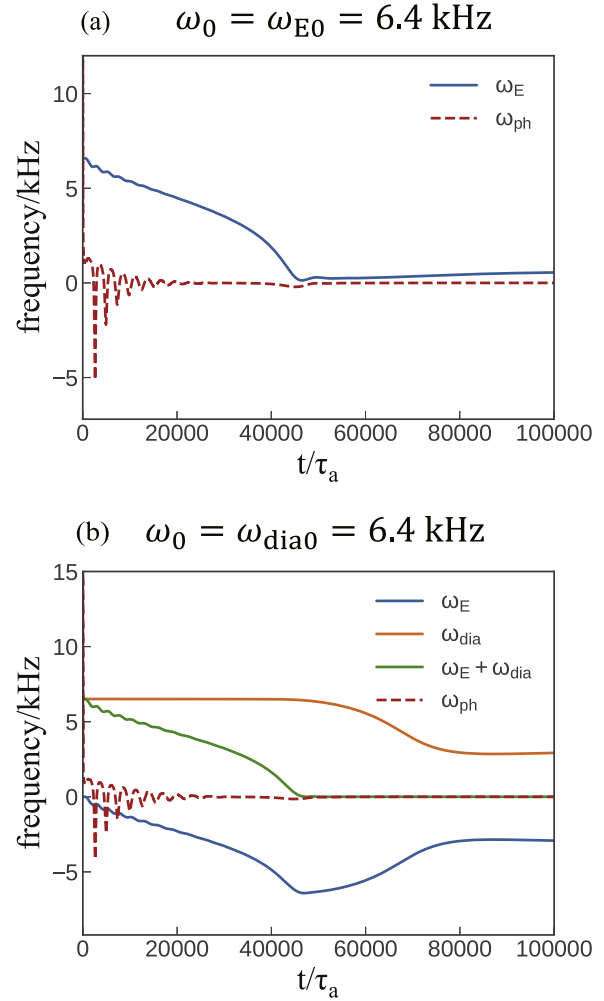
Figure 6. Nonlinear evolution of the island width for $\omega_0 = \omega_{E0} = 6.4$ kHz (solid) and $\omega_0 = \omega_{dia0} = 6.4$ kHz (dashed).

the $\mathbf{E} \times \mathbf{B}$ electric drift flow. The equilibrium $\mathbf{E} \times \mathbf{B}$ flow velocity can be directly obtained by $v_{E0} = \partial\phi_0/\partial r$, and the equilibrium electron diamagnetic flow velocity can be calculated by $v_{dia0} = -\delta\partial p_0/\partial r$, where the subscript 0 is for equilibrium quantities. Therefore, the natural plasma rotation could be obtained by the sum of these two effects. By changing the value of δ, different amplitudes of diamagnetic drift flow can be implemented.

As shown in figure 6, the screening effects of the two types of flow on the RMP penetration are compared. The solid lines are for cases with an equilibrium $\mathbf{E} \times \mathbf{B}$ flow frequency $\omega_{E0} = 6.4$ kHz and diamagnetic flow frequency $\omega_{dia0} = 0$, while dotted lines for $\omega_{dia0} = 6.4$ kHz and $\omega_{E0} = 0$. Thus, for both cases, the natural frequency is $\omega_0 = \omega_{E0} + \omega_{dia0} = 6.4$ kHz. It makes no difference on the penetration threshold, no matter what kind of flow it is, which means that the penetration threshold only depends on the rotation difference between the resonant surface and the RMP. Corresponding to the two penetrated cases in figure 6, the temporal evolutions of the flow frequencies ω_E, ω_{dia}, $\omega_E + \omega_{dia}$ and the frequency of the phase of the island ω_{ph} are illustrated in figure 7. It shows a good agreement for the flow frequency and the phase frequency after mode penetration, indicating that the magnetic island and the flow are coupled in accordance with the frozen-in theorem. For the case ($\omega_{E0} = 6.4$ kHz, $\omega_{dia0} = 0$), the ω_E decreases with time and drops to zero at the moment penetration occurs. For the case ($\omega_{E0} = 0$, $\omega_{dia0} = 6.4$ kHz), since the ω_{dia} is a rigid flow effect that is mainly proportional to the pressure gradient, it does not change at the beginning but starts to decrease as the magnetic island grows, where the pressure gradient is flattened. As a consequence, the ω_E will rotate in the opposite direction to cancel the diamagnetic flow.

When it comes to a larger rotation frequency, the situation is somewhat different. Similar to figure 6, the nonlinear evolution of the island width for a larger natural frequency $\omega_0 = 12.8$ kHz is presented in figure 8. It shows again that the

Figure 7. Temporal evolutions of the phase frequencies ω_{ph} and different flow frequencies ω_E, ω_{dia}, and $\omega_{tot} = \omega_E + \omega_{dia}$. The ω_{ph} is calculated by the partial derivative of the phase of poloidal flux Φ_ψ with respect to time. ω_E and ω_{dia} are the angular frequencies of electric drift and diamagnetic drift flow, respectively.
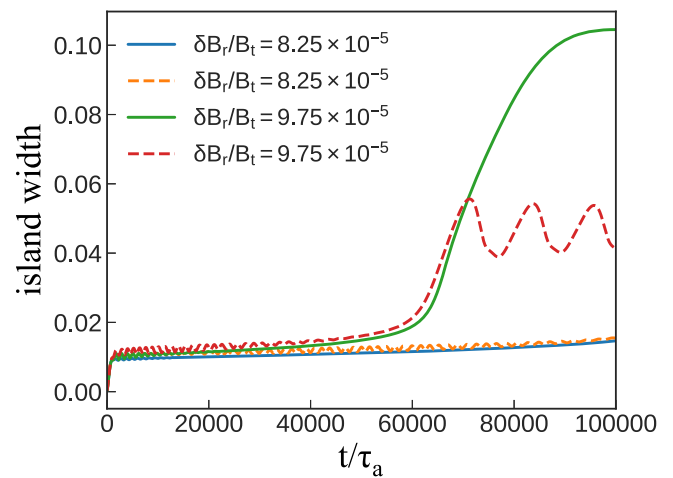
Figure 8. Nonlinear evolution of the island width for $\omega_0 = \omega_{E0} = 12.8$ kHz (solid) and $\omega_0 = \omega_{dia0} = 12.8$ kHz (dashed).
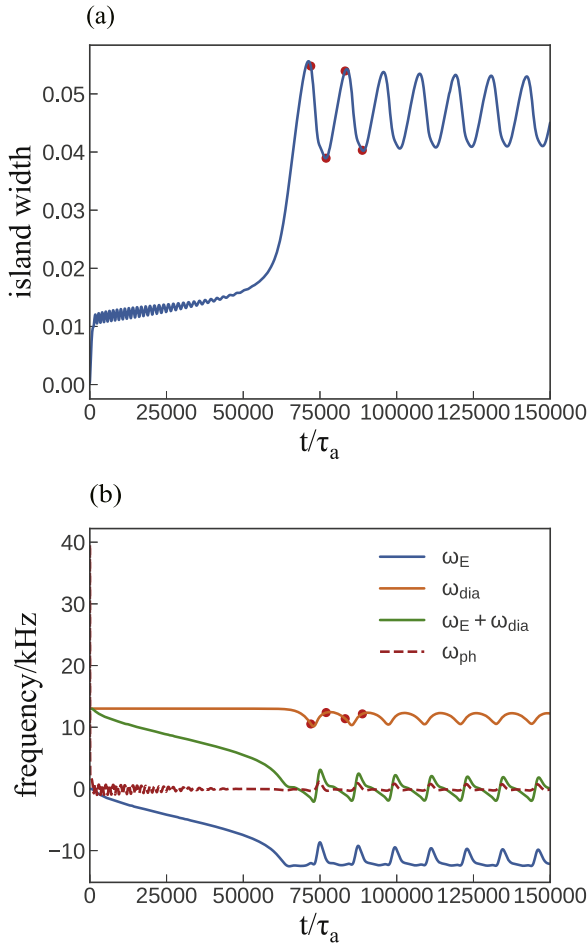
Figure 9. Temporal evolution of the island width and various frequencies for the oscillated case ($\omega_0 = \omega_{\mathrm{dia0}} = 12.8$ kHz, $\delta B_r / B_0 = 9.75 \times 10^{-5}$) in figure 8. Oscillation of ω_{dia} is observed after mode penetration. Four time points $t = 73000$, $t = 77000$, $t = 83200$, and $t = 88800$ are marked by the red circles.

penetration threshold is almost the same. However, there are two differences observed. First, the saturated island width is evidently smaller for the case ($\omega_{\mathrm{E0}} = 0$, $\omega_{\mathrm{dia0}} = 12.8$ kHz) than that of the case ($\omega_{\mathrm{E0}} = 12.8$ kHz, $\omega_{\mathrm{dia0}} = 0$), implying that the diamagnetic flow can drive a stabilizing effect on the magnetic island. Second, an oscillation phenomenon of the magnetic island is discovered after mode penetration. To further analyze this oscillation phenomenon, the island width and flow frequency of the oscillated case in figure 8 are plotted, as shown in figure 9. The periodical oscillation of diamagnetic flow frequency is observed as well in figure 9(b). It should be noted that the oscillation of frequency lags behind the island width a bit, suggesting that the change of island width results in the change of the diamagnetic flow frequency at first. Since the diamagnetic flow is proportional to the pressure gradient, it can be straightforwardly inferred that this phenomenon is related to the change in plasma pressure. To proceed to a further step, the contour plot of the pressure p together with the poloidal magnetic flux ψ is shown in figure 10, corresponding to the four red time points in figure 9. As the magnetic island grows larger ($t = 73000$ and $t = 83200$), the pressure gradient $\nabla_{\parallel} p$

with respect to the magnetic field inside the island becomes larger. For a smaller island width ($t = 77000$ and $t = 88800$), in contrast, $\nabla_{\parallel} p$ is smaller. This modification of the pressure gradient can in return affect the island width by the $\delta \nabla_{\parallel} p$ term in equation (2), leading to the above oscillation phenomenon. To make it more clear, the nonlinear evolutions of the island width and the value of $\nabla_{\parallel} p$ at the resonant surface are plotted in figure 11. It is obviously shown that the island width and pressure gradient exhibit a negative feedback relationship, as discussed above.

In order to further verify our conjecture, the effect of resistivity η is then investigated. For a larger η, it turns out that the oscillation phenomenon disappears and the island width recovers as illustrated in figure 12(a). It can be easily understood through equation (2). Since η is a diffusive term, the effect of $\delta \nabla_{\parallel} p$ term, stabilizing the island and causing the oscillation, can be diffused to some extent with the increasing η, in much the same way as viscosity ν in the vorticity equation stabilizing the oscillation of rotation. In other words, the oscillation phenomenon is a result of the competition of the two terms $\delta \nabla_{\parallel} p$ and $\eta(j - j_{\mathrm{b}})$. For the same reason, a smaller bootstrap current fraction f_{b} can remove the oscillation by making the $\eta(j - j_{\mathrm{b}})$ term larger, shown in figure 12(b). As the ratio of parallel to perpendicular transport coefficients, $\chi_{\parallel} / \chi_{\perp}$ is crucial to the process of pressure evolution, the effects of different $\chi_{\parallel}$ and $\chi_{\perp}$ values are studied. In figures 12(c) and (d), the temporal evolution of the island width is plotted for different $\chi_{\parallel}$ and $\chi_{\perp}$. The results are intuitive, i.e. a smaller $\chi_{\parallel}$ or larger $\chi_{\perp}$ can eliminate the oscillation. This is because a smaller $\chi_{\parallel} / \chi_{\perp}$ can lower the energy transport level along the magnetic field lines, which would reduce the variation of the $\delta \nabla_{\parallel} p$ term when the size of the magnetic island changes.

4. Summary and discussion

The initial value code MDC (MHD@Dalian Code) is upgraded with the capability of two-fluid effects. On the basis of the well-known four-field equations [47], the bootstrap current, parallel and perpendicular transport effects are additionally included. In this work, the numerical simulation of the mode penetration is conducted based on the two-fluid model. The main points can be summarized as follows.

(i) The threshold of mode penetration at zero rotation is explored. It is found that for the classical TM ($f_{\mathrm{b}} = 0$), there is no threshold for mode penetration. In this circumstance, the behavior of the magnetic island is dominated by driven reconnection, i.e. the saturated island width is positively related to the amplitude of RMP. For the NTM ($f_{\mathrm{b}} \neq 0$), on the other hand, a mode penetration-like phenomenon is observed consisting of a driven reconnection regime and an NTM regime. This phenomenon is different from the so-called mode penetration but can be mistakenly defined as mode penetration if not carefully distinguished. It may provide a possible explanation for the finite mode penetration threshold at zero rotation detected in experiments. The
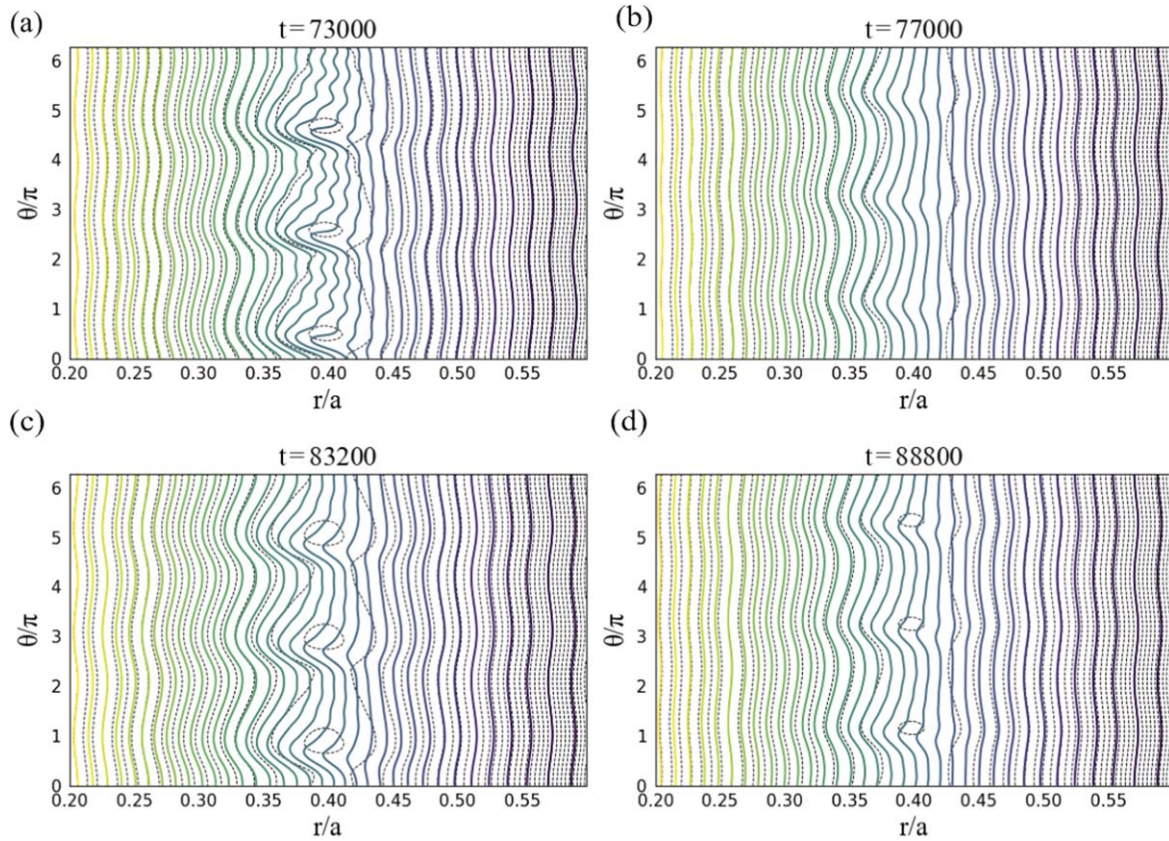
Figure 10. Contour plot of the plasma pressure p (solid lines) and poloidal flux ψ (dotted lines), corresponding to the four red time points marked in figure 9.
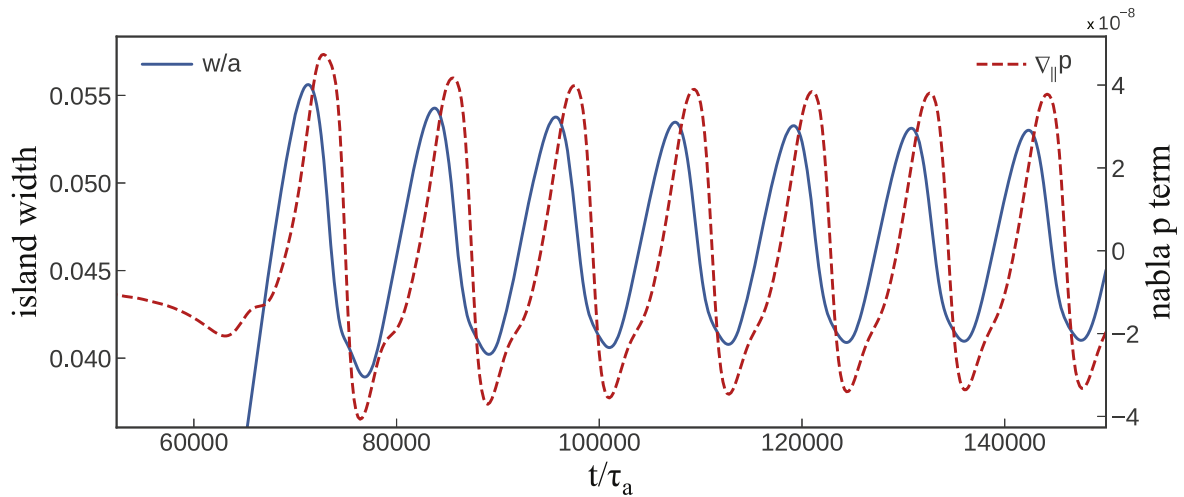

Figure 11. Nonlinear evolution of the island width (solid) and the value of $\nabla_\parallel p$ (dotted) at the resonant surface after mode penetration.

polarization drift, which is an important physics for NTM besides the pressure transport model, is not included in this work. Its role will be investigated in a future study.

(ii) The effect of diamagnetic drift flow on mode penetration is numerically studied. For a smaller diamagnetic drift flow, numerical results show that its influence is almost the same as the electric drift flow with comparable frequency.

However, for a larger diamagnetic drift flow, it can drive a stabilizing effect on the magnetic island through the $\delta\nabla_\parallel p$ term in equation (2). Besides, an oscillation phenomenon of the island width is observed. This oscillation is linked with the change of pressure during the variation of island width. It tends to appear in the high Lundquist number S and high $\chi_\parallel/\chi_\perp$ regime, where the parameter of the advanced tokamak exactly lies.
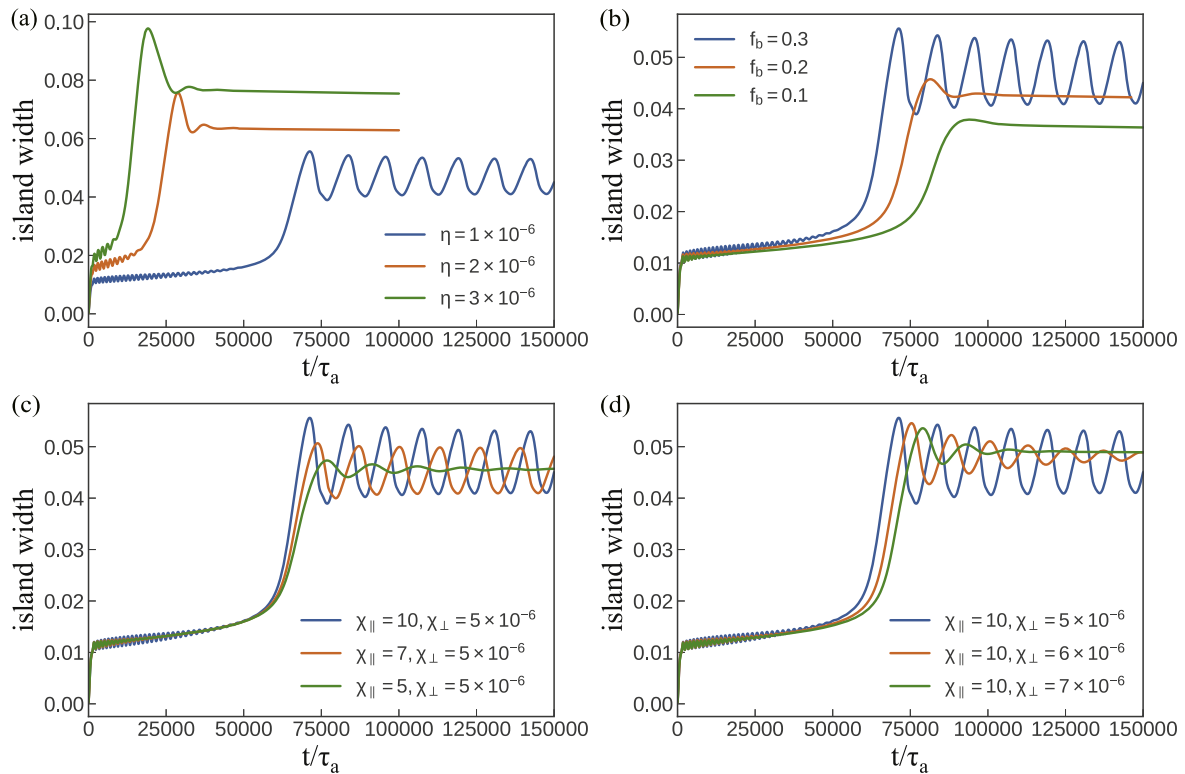
Figure 12. Comparison of island width versus time for different (a) resistivity η, (b) bootstrap current fraction $f_{\rm b}$, (c) parallel transport coefficient $\chi_\parallel$ and (d) perpendicular transport coefficient $\chi_\perp$.

Acknowledgments

ORCID iDs

Weikang TANG (汤炜康) ⓘ https://orcid.org/0000-0002-8406-8349

References

[1] Furth H P, Killeen J and Rosenbluth M N 1963 *Phys. Fluids* **6** 459
[2] Rutherford P H 1973 *Phys. Fluids* **16** 1903
[3] Carrera R, Hazeltine R D and Kotschenreuther M 1986 *Phys. Fluids* **29** 899
[4] Bardóczi L *et al* 2017 *Phys. Plasmas* **24** 056106
[5] Wang Z X, Wei L and Yu F 2015 *Nucl. Fusion* **55** 043005
[6] Zhang W *et al* 2019 *Plasma Phys. Control. Fusion* **61** 075002
[7] La Haye R J 2006 *Phys. Plasmas* **13** 055501
[8] Sauter O *et al* 2010 *Plasma Phys. Control. Fusion* **52** 025002
[9] Maraschek M 2012 *Nucl. Fusion* **52** 074007
[10] Hender T *et al* 1992 *Nucl. Fusion* **32** 2091
[11] Yu Q, Günter S and Finken K H 2009 *Phys. Plasmas* **16** 042301
[12] Buttery R *et al* 1999 *Nucl. Fusion* **39** 1827
[13] Lanctot M *et al* 2016 *Nucl. Fusion* **56** 076003
[14] Lu S S *et al* 2020 *Plasma Phys. Control. Fusion* **62** 125005
[15] Logan N *et al* 2021 *Nucl. Fusion* **61** 076010
[16] Wang Z X, Tang W K and Wei L 2022 *Plasma Sci. Technol.* **24** 033001
[17] Nave M and Wesson J 1990 *Nucl. Fusion* **30** 2575
[18] Wang H H *et al* 2015 *Plasma Sci. Technol.* **17** 539
[19] Wolf R *et al* 2005 *Nucl. Fusion* **45** 1700
[20] Choi W *et al* 2018 *Nucl. Fusion* **58** 036002
[21] Tang W K *et al* 2020 *Nucl. Fusion* **60** 026015
[22] Nelson A O *et al* 2020 *Plasma Phys. Control. Fusion* **62** 094002
[23] Fitzpatrick R 1993 *Nucl. Fusion* **33** 1049
[24] Yu Q and Günter S 2008 *Nucl. Fusion* **48** 065004
[25] Buttery R *et al* 2000 *Nucl. Fusion* **40** 807
[26] Haye R L, Hyatt A and Scoville J 1992 *Nucl. Fusion* **32** 2119
[27] Wang N C *et al* 2014 *Nucl. Fusion* **54** 064014
[28] Wang H H *et al* 2018 *Nucl. Fusion* **58** 056024
[29] Cole A J, Hegna C C and Callen J D 2007 *Phys. Rev. Lett.* **99** 065001
[30] Wang J L, Wang Z X and Wei L 2015 *Phys. Plasmas* **22** 092122
[31] Beidler M T *et al* 2018 *Phys. Plasmas* **25** 082507
[32] Zhang H W *et al* 2021 *Plasma Phys. Control. Fusion* **63** 035011
[33] Becoulet M *et al* 2012 *Nucl. Fusion* **52** 054003
[34] Yu Q, Günter S and Lackner K 2018 *Nucl. Fusion* **58** 054003
[35] Fitzpatrick R 2018 *Phys. Plasmas* **25** 082513
[36] Fitzpatrick R 2018 *Phys. Plasmas* **25** 112505
[37] Hu Q M *et al* 2020 *Nucl. Fusion* **60** 076006
[38] De Bock M F M *et al* 2008 *Nucl. Fusion* **48** 015007

[39] Yu Q, Günter S and Lackner K 2021 *Nucl. Fusion* **61** 036040
[40] Wei L *et al* 2016 *Nucl. Fusion* **56** 106015
[41] Wang J L *et al* 2017 *Nucl. Fusion* **57** 046007
[42] Liu T *et al* 2018 *Nucl. Fusion* **58** 076026
[43] Ye C *et al* 2019 *Nucl. Fusion* **59** 096044
[44] Jiang S *et al* 2022 *Plasma Sci. Technol.* **24** 055101
[45] Han M K *et al* 2017 *Nucl. Fusion* **57** 046019
[46] Wang W *et al* 2018 *Plasma Sci. Technol.* **20** 075101
[47] Hazeltine R D, Kotschenreuther M and Morrison P J 1985 *Phys. Fluids* **28** 2466
[48] Bickerton R J, Connor J W and Taylor J B 1971 *Nat. Phys. Sci.* **229** 110
[49] Strauss H 1977 *Phys. Fluids* **20** 1354
[50] Morrison P J, Tassi E and Tronko N 2013 *Phys. Plasmas* **20** 042109
[51] Kikuchi Y *et al* 2006 *Phys. Rev. Lett.* **97** 085003
[52] Hu Q M *et al* 2012 *Nucl. Fusion* **52** 083011
[53] Tang W K *et al* 2019 *Plasma Sci. Technol.* **21** 065103
[54] Nies R, Reiman A H and Fisch N J 2022 *Nucl. Fusion* **62** 086044